Supporting Information for

Dual-drive acoustic micromixer for rapid nucleation and ultrafast growth of perovskite nanoparticles

Zhifang Liu,[1] Yuwen Lu,[1] Wei Tan,[1, 2] and Guorui Zhu[1 ,2,]*

1. School of Chemical Engineering and Technology, Tianjin University, Tianjin, 300354, China

2. Zhejiang Institute of Tianjin University, Ningbo, Zhejiang, 315201, China

*. Corresponding author. E-mail: zhuguorui@tju.edu.cn

Chip structure

The microfluidic devices were fabricated with standard soft lithography techniques, including SU-8 mold manufacturing, polydimethylsiloxane (PDMS) pouring and plasma bonding. Both microchannels have a depth of 100 μm and a main channel width of 600 μm. The distances between the vortice of sharp edges and the wall are both 300 μm, with an angle of 15∘ and an interval of 300 μm distributed alternately on both sides of the channel. In particular, a groove for bubble trapping was distributed in the middle of every two sharp edges on one side of the S2 microchannel.

In this study, we have designed both trapezoidal and rectangular notch structures for capturing air bubbles. Figure S3 illustrates the effect of flow rate and notch structure on bubble size. It can be observed that bubble size is inversely proportional to flow rate, with bubbles almost completely washed away in the range of flow rates greater than 1000μL/min. Bubbles are less likely to be washed away in a trapezoidal structure than in a rectangular groove.
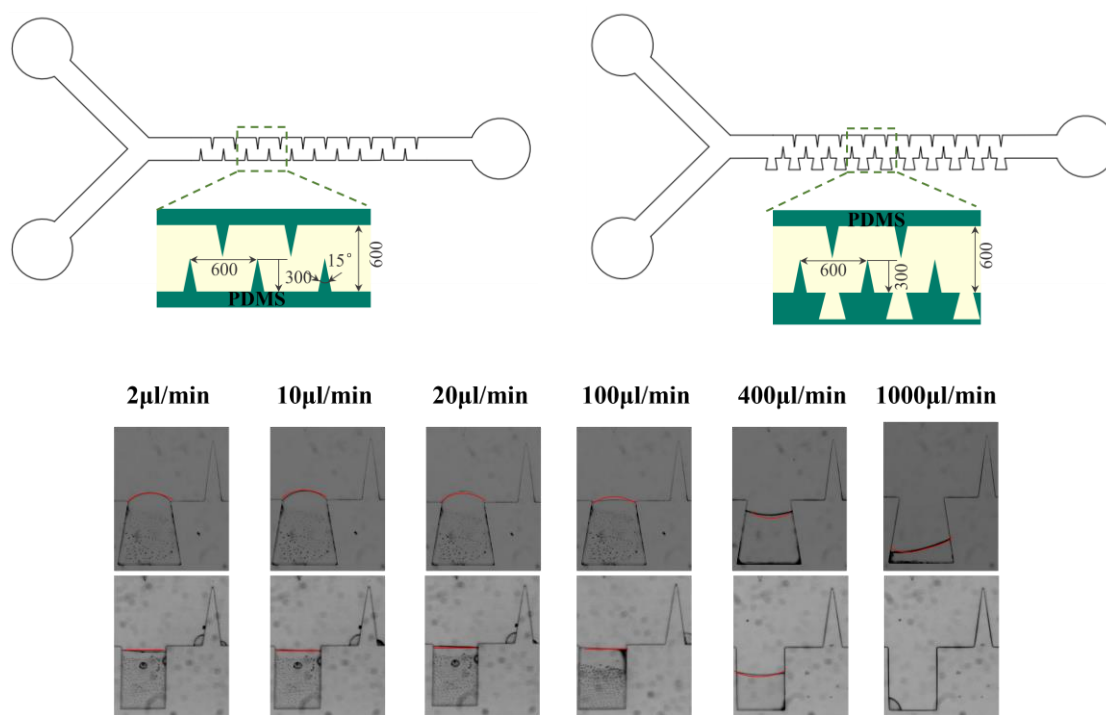
Figure S1. (a) Structural dimensions of the two micromixers. (b) Variation of bubbles with flow in trapezoidal(above) and rectangular(below) fluted structures.

Materials and Methods

Lead bromide (PbBr2, AR, 99.0%, Aladdin, China), cesium bromide (CsBr, metals basis, 99.5%, Aladdin), oleic acid (OA, AR, Sinopharm Chemical Reagent Co., Ltd., China), oleylamine (OLA, C18: 80%–90%, Macklin, China), N,N-dimethylformamide (DMF, absolute, over molecular sieve, Macklin, China), dimethyl sulfoxide (DMSO, absolute, over molecular sieve, Macklin, China), IPA[1] (AR, 99.5%, Macklin, China), Fluorescein Na (Solarbio Life Sciences, China), Polystyrene particles (20 μm, BaseLine Chromtech Research Center, China), poly-dimethylsiloxane (PDMS).All reagents were used as received.

The precursor solution 1 was prepared by dissolving CsBr (0.8 mmol), PbBr2 (0.8 mmol), OAm (1 ml), and OA (2 ml) with 20 ml dried DMF. IPA solution was employed as the precursor solution 2. The precursor solutions 1 and 2 were pumped into the microchannel at a ratio of 1:10, with a total flow rate ranging from 100 to 3000 µL/min. The as-obtained colloidal solution of CsPbBr3 NCs flowed into a 20 ml sample bottle and was left to stand for 1 h to remove the extremely large nanoparticles. The

precipitate at the bottom of the sample bottle was discarded, washed with triple ethyl acetate to remove any unreacted ligands, and centrifuged at 7000 rpm for five minutes. Retaining the supernatant for further characterization. The properties were characterized using the X-ray diffraction (XRD), Horiba Fluoromax-4 Spectrofluorometer, Ultraviolet-Visible (UV-Vis, Shimadzu, Japan), and JEM-2100 transmission electron microscope (JEOL, Japan).

In order to select suitable solvents, six groups of solvents commonly found in the literature were initially identified. The target product, a chalcogenide, exhibits green fluorescence under 365 nm UV irradiation. As illustrated in Figure S2, the combination of DMF-TL and DMF-IPA is more complex. Given the strong toxicity of TL, the final choice was DMF-IPA.
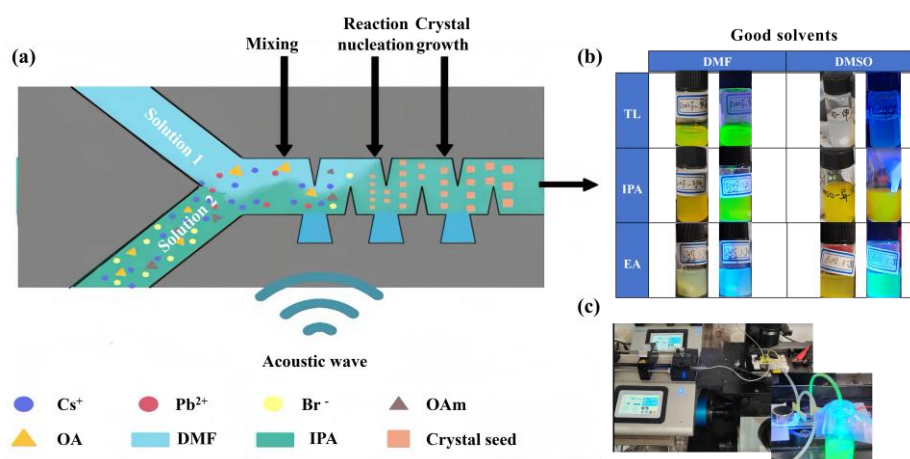

Figure S2. (a) The schematic of experimental setup for the continuous synthesis of CsPbBr3 NCs; (b) Selection of solvents; (c) Construction of the experimental platform.

Mixing mechanism

Acoustic streaming of sharp edge: When alternating electrical signals drive the piezoelectric transducer, sound waves propagate along the glass substrate, which forces the sharp edge to produce a pair of counter-rotating vortices around the tip, known as acoustic streaming [2].

Acoustic streaming of bubble: When the channel is filled with solutions, the grooves in the side walls trap bubbles due to surface tension. When driven by an acoustic transducer, the membrane of the trapped bubble begins to oscillate. Oscillations generate fluctuations in the velocity and pressure of the surrounding fluid, resulting in a strong recirculating flow pattern throughout the liquid near the bubble [3]. It is most efficient when the bubble is excited at its resonance frequency. The resonance frequency, f, of an acoustically driven bubble can be estimated by the small-amplitude behavior of the Rayleigh–Plesset equation [4].

$$f^2 = \frac{1}{4\rho\pi^2 a^2}\left\{3k\left(p + \frac{2\sigma}{a}\right) - \frac{2\sigma}{a}\right\}$$

where r is the density of the liquid (kg/m3), s is the surface tension of solution (N/m), k is the polytropic exponent for a bubble containing air, p is the fluidic pressure (N/m/), and a is the radius of the bubble (m).

Horizontal vortex: In sharp edges and grooves structures, the change in the direction of fluid flow leads to the separation of the boundary layer and formation of vortex in the horizontal plane. The intensity of horizontal vortex is related to Reynolds number[5].

$$Re = \frac{\rho u D_h}{\mu}$$

where, D_h is the hydraulic diameter of microchannels, u is the average flow velocity, μ is the dynamic viscosity, ρ is the fluid density.

Flow characteristics of S2

There is a negative correlation between the size of the micro-vortices and the input flow rate due to the suppression of acoustic micro-vortices by the mainstream. Furthermore, the vortices generated at the resonance frequency decay more rapidly. The blue region on the left side corresponds to the bubble resonance frequency. It can be observed that the vortex height produced by the bubble decreases by 40.8% in the flow rate range of 2-50 μL/min, while the vortex height produced by the sharp edge decreases by only 10.38%. A similar outcome was observed in the pink region on the right side, where the vortex heights generated by sharp edges and bubbles decreased by 32.16% and 23.11%, respectively at the sharp corner resonance frequency.
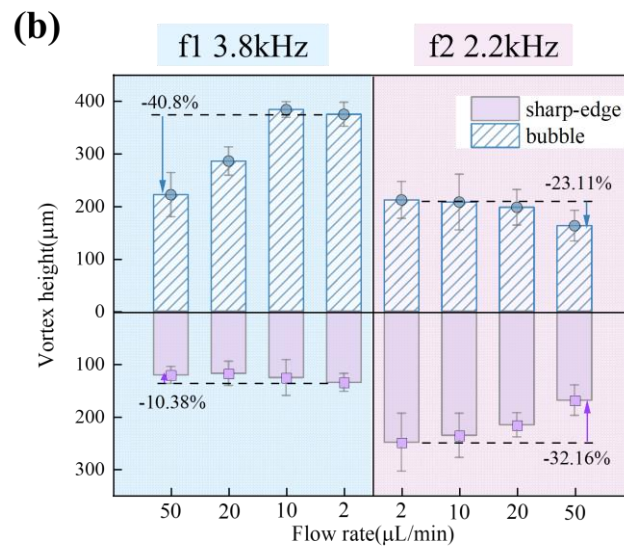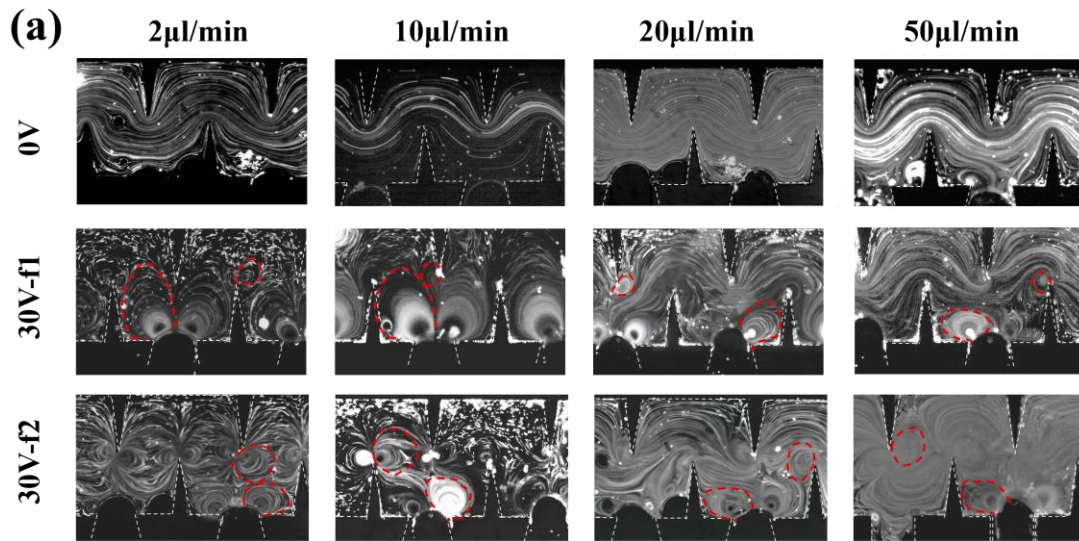
Figure S3. (a) Flow patterns obtained from fluorescent particle tracer experiments in S2 microchannels. The red dotted line indicates the position of the vortex. (b) variation patterns of vortex heights generated by sharp edges and bubbles with flow rate in different frequency of the input signal.

Mixing performance

Figure S4a illustrate the variation in the mixing index at the outlets of S1 and S2 microchannels for the two inlet fluids being a 1 to 1 flow ratio.

When the piezoelectric transducer is turned off, the fluid interface is clear in the flow range of Q < 20μL/min, indicating that almost no mixing happened. This mixing relies on slow molecular diffusion based on laminar flow. The smaller the flow rate, the longer fluid stays in the channel, increasing the time for molecular diffusion, and therefore the mixing index decreases slightly in this range (Q<20μL/min). Complete mixing is achieved in both microchannels due to the disturbing effect of strong inertial vortices on the fluid at the sharp edges(Q>1000μL/min).

When the piezoelectric transducer is turned on, the acoustic flow generated by the sharp edges vibration ensures complete mixing of the solution in both channels, resulting in a uniform green solution (Figure S4b, c). The mixing index is consistently above 0.8.

Figure S4d illustrate the variation in the mixing index at the outlets of S1 and S2 microchannels for the two inlet fluids being a 1 to 10 flow ratio.

When the piezoelectric transducer is turned off, similar to the 1:1 flow ratio, mixing relies on slow molecular diffusion. The fluid interface is clear and essentially no mixing in the flow range of Q<20μL/min. When 100μL/min < Q<1000μL/min, only the horizontal vortex generated by one side of the sharp edge disturbs the fluid and the mixing index is slightly lower in S1. In contrast, S2 has a higher mixing index.

When the piezoelectric transducer is turned on, the acoustic flow is suppressed by the main flow (20μL/min < Q < 1000μL/min) and only one set of sides works and the mixing index is significantly reduced in S1. In contrast, in addition to a set of sidewalls with sharp edges, there are vortices generated by surface vibrations of the bubbles captured by the grooves used to mix the fluid in S2. This results in complete mixing throughout the entire range of flow rates tested in the experiments, with mixing index is consistently above 0.8.
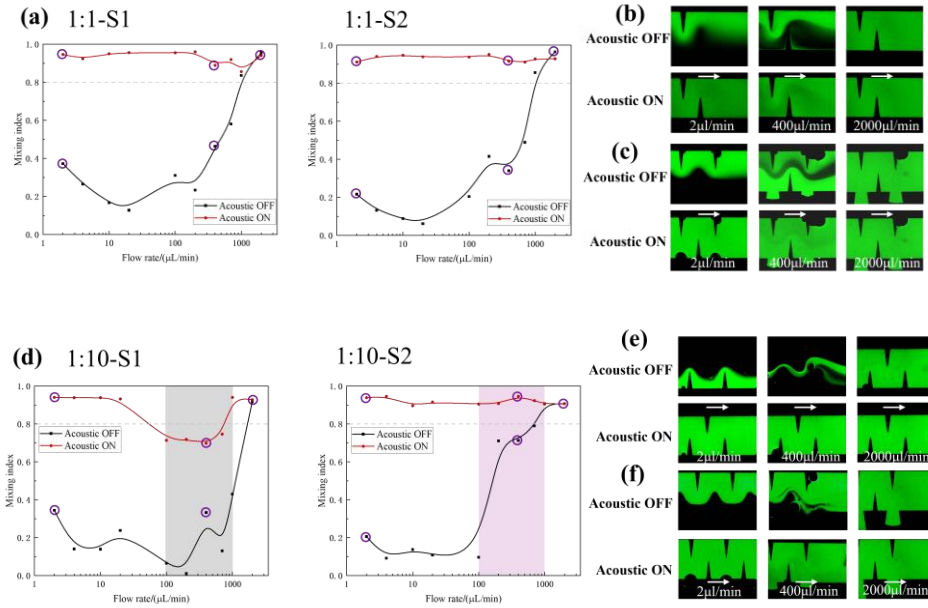
Figure S4. Mixing performance of S1 and S2 at different flow rates when the piezoelectric transducer is turned off or on. And the flow rate of the inlet fluids is (a)1:1; (b)1:10; Purple circles represent fluorescent pictures at the outlet of (b) (e) S1 and (c) (f)S2 when the piezoelectric transducer is turned off and on respectively at the marked flow rate. The sampling locations of the fluorescence images are all at the outlet of channel.

Mixing time

Mixing time is defined by $t = L/u$, where L is the mixing length and u is the average velocity of the fluid along the direction of the channe[16]. The mixing length is defined as the distance from the last unmixing point to the first fully mixing point at the center of the channel. For example, with the input voltage of 20Vpp and the flow rate of 10μL/min, the mixing length is 316μm shown in Fig S5. The corresponding mixing time was 10.29ms. The mixing time under all flow rates tested in the experiment is shown in Fig S5. As the flow rate increases, the mixing time shows a clear decreasing trend.
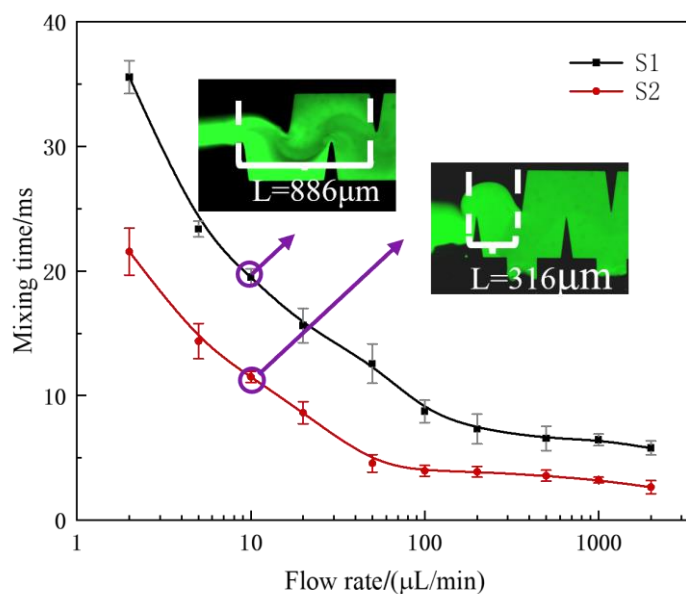
Figure S5. Relationship between mixing time and flow rate of S1 and S2 micromixers at a flow ratio of 1:10 and a fixed driving voltage (20Vpp).

Mixing of different scenarios

Figure S8 illustrates the mixing of different working conditions for synthetic chalcogenide nanoparticles. The different working conditions correspond to different mixing levels, which affect the degree of supersaturation and hence particle nucleation.
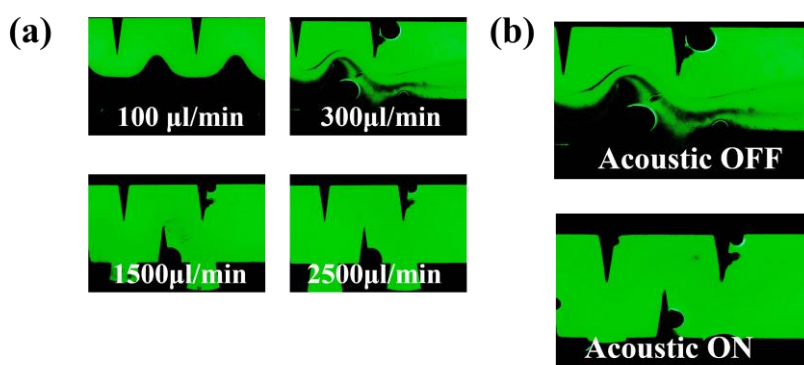

Figure S6. (a) Mixing of fluorescent solution and DI water at different flow rates; (b) Mixing of fluorescent solution and DI water with and without acoustic field excitation at a total flow rate of 300 µL/min.

Comparison with other microreactors

Microreactors have made significant advancements in materials synthesis; however, three crucial limitations restrict their applicability in this field. Firstly, some of the reaction processes are inherently cumbersome to operate. In addition to crystallization using the polarity difference between the two solvents, there is also cooling crystallization using the temperature difference, which requires the temperature of the reactor to be regulated using a heated platform, oil bath, etc., and it is not possible to realize the synthesis at room temperature. [7-11] Zhan et al. synthesized nanocrystals using flow-focusing microreactors at room temperature, but the operation process required the simultaneous operation of three syringe pumps, which was cumbersome.[12] The methodology described in this paper can be performed at room temperature and is relatively straightforward to execute.

Secondly, microreactors for passive mixing in materials synthesis are of the U-tube, [13] spiral tube, [14] and similar varieties. Their mixing performance is highly dependent on the flow rate and poorly tunable. Devices that rely on active mixing techniques, as demonstrated by Ng et al [15], employ high-frequency ultrasonics (1.06 MHz) to drive acoustic flow through a silicon plate mixer, achieving millisecond-scale mixing. However, acoustic flow-enhanced micromixers operate at low flow rates, for example, 1.1 ml/min. Li et al.[16] employ ultrasonic cavitation within the channel to achieve rapid mixing, but there are limitations in terms of instability in the reaction process. In this paper, we propose a novel approach that combines active acoustic mixing generated by sharp corners and bubbles with inertial mixing due to sharp corners and grooves. Both highly tunable rapid mixing and efficient operation over a wide flow range are achieved.

Last, microreactors are at significant risk of fouling and clogging due to the small characteristic channel size. In this manuscript, the sharp corners and bubbles exhibit significant oscillatory behavior within the fluid medium, resulting in the generation of substantial shear forces. This mechanical action not only enhances the mixing and mass transfer processes but also facilitates the disruption and disaggregation of particle aggregates, enabling the separation of particles deposited on the channel walls.[17, 18]

In conclusion, the micromixer designed in this manuscript is capable of efficient mixing in a matter of milliseconds and can facilitate the synthesis of products at room temperature. The reaction process is highly controllable. Furthermore, the incorporation of an acoustic field not only facilitates enhanced mixing and mass transfer but also generates substantial shear stresses, which effectively prevents particle aggregation and mitigates the risk of fouling.

1 X. Cheng, Y. Zhai, X. Wang, X. Cao, D. Guan, H. Zhang, Q. Zhu, S. Fang and L. Wang, *Journal of Luminescence*, 2024, **271**.

2 P.-H. Huang, Y. Xie, D. Ahmed, J. Rufo, N. Nama, Y. Chen, C. Y. Chan and T. J. Huang, *Lab on a Chip*, 2013, **13**.

3 A. Ozcelik, D. Ahmed, Y. Xie, N. Nama, Z. Qu, A. A. Nawaz and T. J. Huang, *Analytical Chemistry*, 2014, **86**, 5083-5088.

4 D. Ahmed, X. Mao, J. Shi, B. K. Juluri and T. J. Huang, *Lab on a Chip*, 2009, **9**.

5 G. Tomaras, C. R. Kothapalli and P. S. Fodor, *Micromachines*, 2022, **13**.

6 X. Li, Z. He, C. Li and P. Li, *Analytica Chimica Acta*, 2021, **1172**.

7 I. G. Koryakina, M. Naumochkin, D. I. Markina, S. A. Khubezhov, A. P. Pushkarev, A. A. Evstrapov, S. V. Makarov and M. V. Zyuzin, *Chemistry of Materials*, 2021, **33**, 2777-2784.

8 Z. Zhang, Y. Liu, C. Geng, S. Shi, X. Zhang, W. Bi and S. Xu, *Nanoscale*, 2019, **11**, 18790-18796.

9 I. Lignos, S. Stavrakis, G. Nedelcu, L. Protesescu, A. J. deMello and M. V. Kovalenko, *Nano Letters*, 2016, **16**, 1869-1877.

10 H. Ma, L. Pan, J. Wang, L. Zhang and Z. Zhang, *Chinese Chemical Letters*, 2019, **30**, 79-82.

11 X. Tang and F. Yang, *Lab on a Chip*, 2022, **22**, 2832-2843.

12 Z. Wei, Y. Chen, P. Lin, Q. Yan, Y. Fan and Z. Cheng, *Journal of Materials Science*, 2019, **54**, 6841-6852.

13 Y. Geng, H. Lv, S. Xu and C. Geng, *Nanoscale*, 2023, **15**, 6371-6378.

14 W. Xing, S. Zhang, R. An, W. Bi, C. Geng and S. Xu, *Nanoscale*, 2021, **13**, 19474-19483.

15 C. K. Ng, H. Deng, H. Li, W. Yin, T. Alan and J. J. Jasieniak, *Journal of Materials Chemistry C*, 2021, **9**, 313-321.

16 M. Li, Z. Liu, W. Yao, C. Xu, Y. Yu, M. Yang and G. Chen, *Chinese Journal of Chemical Engineering*, 2023, **59**, 32-41.

17 Z. Dong, D. Fernandez Rivas and S. Kuhn, *Lab on a Chip*, 2019, **19**, 316-327.

18 Z. Dong, A. P. Udepurkar and S. Kuhn, *Ultrasonics Sonochemistry*, 2020, **60**.